

High-field metamagnetism in the antiferromagnet CeRh₂Si₂

W. Knafo¹, D. Aoki², D. Vignolles¹, B. Vignolle¹, Y. Klein¹, C. Jaudet¹, A. Villaume², C. Proust¹, and J. Flouquet²

¹ *Laboratoire National des Champs Magnétiques Intenses, UPR 3228, CNRS-UJF-UPS-INSA, 143 Avenue de Rangueil, 31400 Toulouse, France. and*

² *Institut Nanosciences et Cryogénie, SPSMS, CEA-Grenoble, 17 rue des Martyrs, 38054 Grenoble, France.*

A study of the antiferromagnet CeRh₂Si₂ by torque, magnetostriction, and transport in pulsed magnetic fields up to 50 Tesla and by thermal expansion in static fields up to 13 Tesla is presented. The magnetic field-temperature phase diagram of CeRh₂Si₂, where the magnetic field is applied along the easy axis **c**, is deduced from these measurements. The second-order phase transition temperature T_N and the first-order phase transition temperature $T_{1,2}$ ($= 36$ K and 26 K at zero-field, respectively) decrease with increasing field. The field-induced antiferromagnetic-to-paramagnetic borderline H_c , which equals 26 T at 1.5 K, goes from first-order at low temperature to second-order at high temperature. The magnetic field-temperature phase diagram is found to be composed of (at least) three different antiferromagnetic phases. These are separated by the first-order lines $H_{1,2}$, corresponding to $T_{1,2}$ at $H = 0$, and $H_{2,3}$, which equals 25.5 T at 1.5 K. A maximum of the T^2 -coefficient A of the resistivity is observed at the onset of the high-field polarized regime, which is interpreted as the signature of an enhanced effective mass at the field-induced quantum instability. The magnetic field dependence of the A coefficient in CeRh₂Si₂ is compared with its pressure dependence, and also with the field dependence of A in the prototypal heavy-fermion system CeRu₂Si₂.

PACS numbers: 72.15.Qm, 75.30.Mb, 75.50.Ee

I. INTRODUCTION

CeRh₂Si₂ is a heavy-fermion antiferromagnet, crystallizing in the ThCr₂Si₂ tetragonal structure, which can be driven to a magnetic instability either by applying pressure¹ or magnetic field^{2,3}. It exhibits a second-order antiferromagnetic transition at the Néel temperature $T_N = 36$ K and a first-order phase transition at $T_{1,2} = 26$ K^{4,5}. For temperatures $T_{1,2} \leq T \leq T_N$, the moments on the Ce sites order antiferromagnetically with wavevector $(1/2, 1/2, 0)$. Below $T_{1,2}$ the antiferromagnetic structure is modified, the intensity of the $(1/2, 1/2, 0)$ Bragg peak being strongly reduced while an additional $(1/2, 1/2, 1/2)$ Bragg peak suddenly develops⁵. De Haas - van Alphen experiments on this system at ambient pressure were interpreted in terms of localized f -electrons⁶. Application of hydrostatic pressure induces a quantum phase transition to a paramagnetic Fermi liquid regime at a critical pressure of around 11 kbar¹ and unconventional superconductivity emerges in the vicinity of the quantum phase transition below a critical temperature going up to $T_{SC}^{max} \approx 0.4$ K^{7,8}. Above 11 kbar, an itinerant description of the f -electrons was proposed from studies of the Fermi surface⁶. In Ref. 2 and 3, the application of a magnetic field along the easy-axis **c** was found to induce two successive first-order transitions, around $H_c \simeq 26$ T, between the low-field antiferromagnetic phase and a high-field polarized paramagnetic regime. At the metamagnetic transition, the magnetization jumps in two successive steps from 0.2 to $1.6 \mu_B/\text{Ce}$ (Ref. 2 and 3).

In this article, we present a study of the properties of CeRh₂Si₂ (at ambient pressure) in high magnetic fields

applied along the easy axis **c**. Torque, magnetostriction, and transport measurements have been carried out in pulsed magnetic fields up to 50 T, and thermal expansion measurements have been performed in static fields up to 13 T. This study enabled us to characterize precisely the magnetic field-temperature phase diagram of the system. We found that the transition temperatures T_N and $T_{1,2}$ decrease with increasing magnetic field. The antiferromagnetic-to-paramagnetic polarization at the magnetic field H_c , which is a second-order transition at high temperature, becomes a first-order transition at low temperature where $\mu_0 H_c$ equals 26 T at 1.5 K. Below 20 K, an additional first-order anomaly develops at a magnetic field $\mu_0 H_{1,2}$, which equals 25.5 T at 1.5 K. These transition lines imply that the magnetic field-temperature phase diagram of CeRh₂Si₂ is composed of (at least) three antiferromagnetic phases. Fits of the low temperature resistivity show a strong and sharp enhancement of the quadratic coefficient $A(H)$ at the transition to the polarized regime. As well as antiferromagnetic fluctuations probably govern the pressure-induced criticality, ferromagnetic fluctuations might play a role at the field-induced instability. We compare the magnetic-field induced instability and previous studies of the pressure-induced instability in CeRh₂Si₂. Assuming that A is proportional to the square of the average effective mass, which is dressed by the magnetic fluctuations, the magnetic field- and pressure-driven enhancements of the mass are discussed. Finally, the properties of CeRh₂Si₂ are compared with those of the canonical example CeRu₂Si₂ of heavy-fermion metamagnetism.

Experimental details are given in Section II. The

(H, T) magnetic phase diagram inferred from our resistivity, torque, and thermal expansion measurements is presented in Section III. Thermal expansion, magnetostriction, torque, and resistivity data are shown and analyzed in Sections IV, V, and VI. In Section VII, we concentrate on the magnetic field-dependence of the quadratic resistivity term A , which is compared with its pressure-dependence and with the magnetic-field dependence of A in CeRu_2Si_2 .

II. EXPERIMENTAL DETAILS

Single-crystalline CeRh_2Si_2 samples were grown by the Czochralski technique in a tetra-arc furnace. Their residual resistivity ratios of ≈ 60 give evidence for the high quality of the crystals. Torque, magnetostriction, and transport experiments were performed up to 50 T at the pulsed magnetic field facility at the LNCMI-Toulouse. Thermal expansion measurements were made in static magnetic fields up to 13 T. Torque measurements were performed using a commercial piezoresistive micro-cantilever developed by Seiko Instruments Incorporated. The sample was glued with Apiezon N grease to the cantilever. A one-axis rotating sample holder allowed a small angle θ to be varied between the \mathbf{c} direction and the magnetic field at ambient temperature. The variation of the piezoresistance of the cantilever was measured with a Wheatstone bridge with an AC excitation at a frequency of 70 kHz. Magnetostriction and thermal expansion were measured along the \mathbf{c} -axis using commercial strain gages from the company Kyowa[®]. A Wheatstone bridge allowed us to measure the difference between the variation of the length of the sample and a reference one (silicon). Magnetostriction and thermal expansion were measured at frequencies of 60 kHz and 20 Hz, respectively. For the resistance measurement, a current excitation of 10 mA at 60 kHz was applied along the \mathbf{a} -axis. The voltage (and a reference signal) was digitized using a high-speed digitizer and post-analyzed to perform the phase comparison. While three samples from the same batch have been measured and give similar results, the data presented here correspond to the sample which has the best geometric factor. Tiny and non-reproducible variations of the out-of-phase signal between two magnetic field pulses led to additional offsets in the resistance versus field data. These offsets were corrected so that the zero-field resistance from each resistance versus field data at a particular temperature corresponds to the resistance versus temperature data measured at zero-magnetic field. For all measurements, the magnetic field \mathbf{H} was applied along \mathbf{c} (with a small additional angle for the torque). Torque and magnetostriction measurements were performed in a longer-pulse magnet (55 ms of rising field and 300 ms of falling field) than the resistivity measurements (26 ms of rising field and 110 ms of falling field). We show only data collected during the decreasing field part of the magnetic field pulse.

III. MAGNETIC FIELD-TEMPERATURE PHASE DIAGRAM

Fig. 1 shows the magnetic field-temperature phase diagram of CeRh_2Si_2 , for $\mathbf{H} \parallel \mathbf{c}$, constructed from our resistivity, torque, and thermal expansion measurements presented in Sections IV, V, and VI. The antiferromagnetic phase, which develops at zero-field below $T_N = 36$ K, is destabilized in magnetic fields H higher than H_c , which equals 26 T at $T = 1.5$ K. H_c corresponds to a field-induced transition to a paramagnetic polarized regime with a strong polarization of the Ce moments^{2,3}. The antiferromagnetic-to-paramagnetic borderline T_N (or equivalently H_c) goes from second-order above ≈ 20 K (and below 24 T) to first-order below ≈ 20 K (and above 24 T). Inside the antiferromagnetic phase two different magnetic transitions correspond to the first-order transitions at $T_{1,2}$ (or equivalently $H_{1,2}$) and $H_{2,3}$. They separate at least three antiferromagnetic phases, noted here AF1, AF2, and AF3. The transition temperature $T_{1,2}$, which equals 26 K at zero-magnetic field (or equivalently the magnetic field $H_{1,2}$), separates the antiferromagnetic phases AF1 and AF2. Both T_N and $T_{1,2}$ decrease with increasing magnetic field. The transition line $H_{2,3}$ corresponds to a field-induced transition between the phases AF2 and AF3, this last phase being stable in a very narrow field-range of about 0.5 T. Torque measurements (see Section V) show that $H_{2,3}$ and H_c , which are distinct at low temperature, merge at about (24 T, 20 K). Our data are compatible with the presence of a critical point at around (24 T, 20 K) where all the antiferromagnetic transition lines would merge. However, the temperature uncertainty and the limited resolution of our experiments in pulsed fields (see

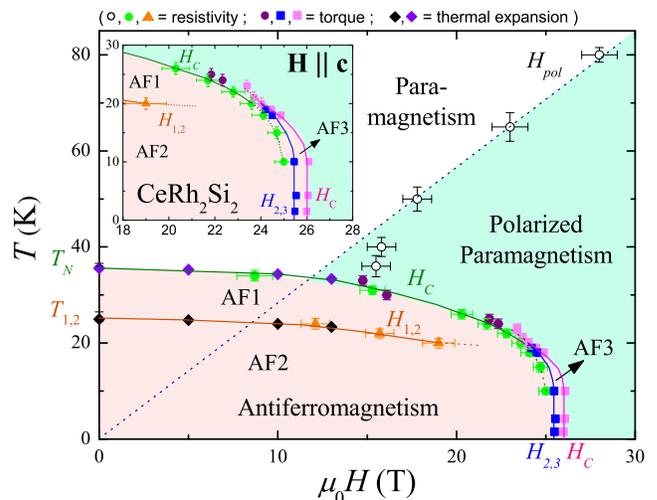


FIG. 1. (Color online) Magnetic field-temperature phase diagram of CeRh_2Si_2 , with $\mathbf{H} \parallel \mathbf{c}$, obtained from resistivity, torque, and thermal expansion. The insert focuses on the low-temperature part of the phase diagram.

Sections IV, V, and VI) do not allow us to conclude if this critical point really exists. Further measurements in static high magnetic fields would be necessary to check more carefully how the different transition lines behave in the proximity of the point (24 T, 20 K) and to test if they merge in a unique critical point. Finally, the high-temperature part of the phase diagram is characterized by a crossover at a magnetic field H_{pol} , defined here using resistivity data (see Section VI), between the low-field antiferromagnetically correlated phase and the high-field polarized phase. H_{pol} increases linearly with T or, equivalently, the characteristic temperature T_{pol} of the high-field polarized state is proportional to H .

IV. THERMAL EXPANSION AND MAGNETOSTRICTION

The temperature dependence of the thermal expansion coefficient $\alpha_c = 1/L_c \times \partial L_c / \partial T$, where L_c is the length of the sample along c , is plotted in Fig. 2 for $20 \leq T \leq 40$ K and magnetic fields $\mathbf{H} \parallel \mathbf{c}$ of 0 T, 5 T, 10 T, and 13 T. Thermal expansion at zero-magnetic field indicates the presence of two phase transitions, a step-like anomaly in $\alpha_c(T)$ is found at the second-order phase transition temperature $T_N = 35.5 \pm 0.1$ K (defined at the extremum of slope of $\alpha_c(T)$) and a symmetric negative peak is found at the first-order transition temperature $T_{1,2} = 25 \pm 0.1$ K (defined at the minimum of $\alpha_c(T)$)⁹. Our zero-field data are in good agreement with previous thermal expansion^{10,11} and specific heat measurements¹², which also indicated the second-order nature of T_N and the first-order nature of $T_{1,2}$ (see also [9]). However, the relative change in length ($\Delta L_c / L_c \simeq 1.7 \times 10^{-4}$) between 5 K and T_N corresponding to the zero-field thermal expansion coefficient α_c plot-

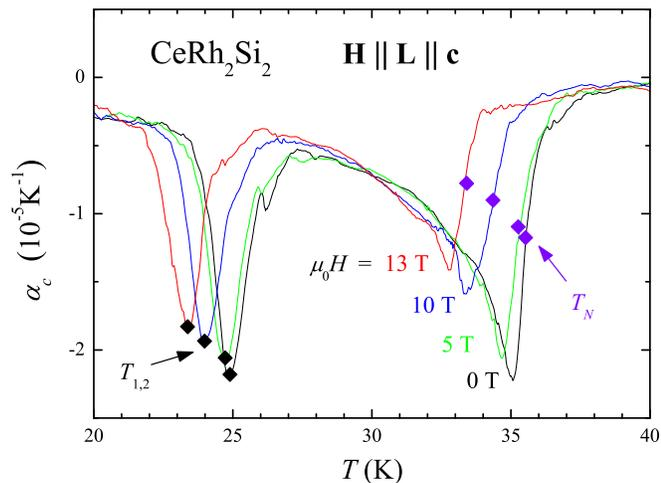


FIG. 2. Thermal expansion coefficient versus temperature of CeRh_2Si_2 measured for magnetic fields $\mu_0 H = 0$ T, 5 T, 10 T, and 13 T applied along \mathbf{c} .

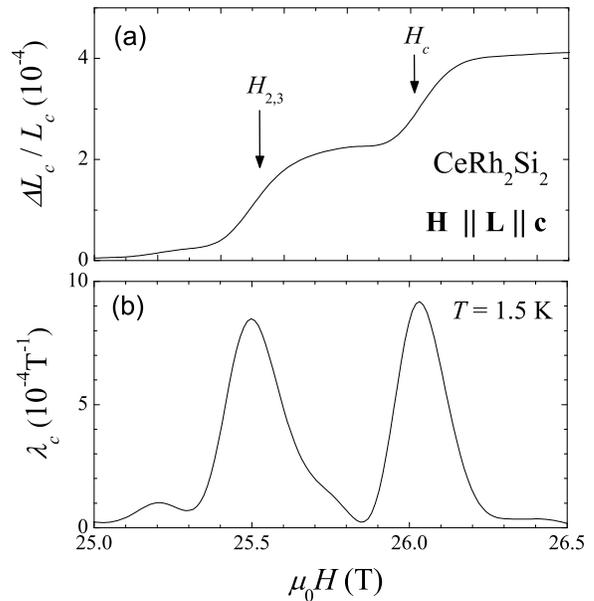


FIG. 3. (Color online) Magnetic field-dependence at $T = 1.5$ K and for $\mathbf{H} \parallel \mathbf{c}$, (a) of the relative length $\Delta L_c / L_c$ of CeRh_2Si_2 and (b) of the related magnetostriction coefficient λ_c .

ted in Fig. 2 is 30 % smaller than the variation of around 2.5×10^{-4} reported using absolute capacitive dilatometry technique^{2,10}. The strain gauge is thus not perfectly coupled to the sample. The efficiency of the coupling is estimated to 70 %. For this reason, the anomalies in $\alpha_c(T)$ reported here at T_N and $T_{1,2}$ are smaller than those from Ref. 10 and 11. As shown in Fig. 2, both T_N and $T_{1,2}$ decrease when a magnetic field is applied along \mathbf{c} . Since the anomalies at T_N and $T_{1,2}$ in $\alpha_c(T)$ are both negative, the Ehrenfest and Clapeyron relations respectively imply that, in magnetic fields $0 \leq \mu_0 H \leq 13$ T parallel to \mathbf{c} , uniaxial pressures applied along \mathbf{c} would decrease both T_N and $T_{1,2}$.

Fig. 3 (a) shows a plot of the magnetic field-variation ($\mathbf{H} \parallel \mathbf{c}$) of $\Delta L_c / L_c$ measured at $T = 1.5$ K. A two-step like increase of $\Delta L_c / L_c$ is induced at the first-order transitions $H_{2,3} \simeq 25.5$ T and $H_c \simeq 26$ T leading to two well-defined peaks in the magnetostriction coefficient $\lambda_c = 1/L_c \times \partial L_c / \partial (\mu_0 H)$ (Fig. 3 (b), see also [9]). The two steps in length variation $(\Delta L_c / L_c)_1 \simeq (\Delta L_c / L_c)_2 \simeq 2 \times 10^{-4}$ measured at $H_{2,3}$ and H_c recall those, equal to $\Delta M_1 \simeq \Delta M_2 \simeq 0.7 \mu_B$, observed in the magnetization at $H_{2,3}$ and H_c (Ref. 2 and 3). Taking into account the 30 % reduction in sensitivity of the length variation, we can estimate the real length variations at $H_{2,3}$ and H_c by $(\Delta L_c / L_c)_{1,2}^{real} \simeq 3 \times 10^{-4}$.

V. TORQUE

Fig. 4 shows a plot of the field-derivative of the torque versus magnetic field of CeRh_2Si_2 at temperatures be-

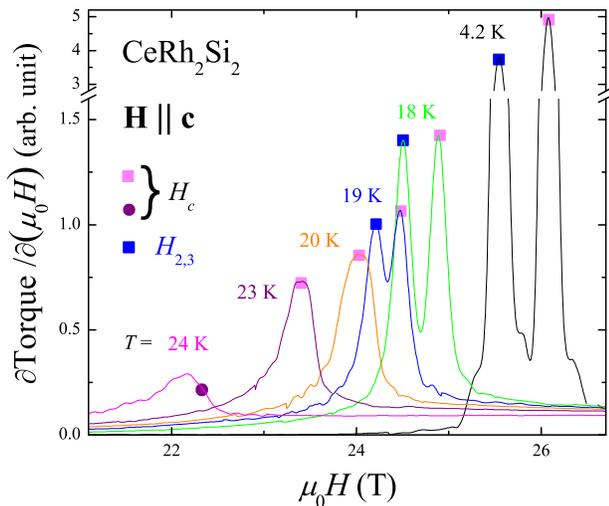


FIG. 4. (Color online) Magnetic field-derivative of the torque in CeRh_2Si_2 versus magnetic field for temperatures $T \leq 24$ K and magnetic fields along \mathbf{c} .

tween 4.2 K and 24 K. The torque signal is proportional to $MH\sin\theta$ where M is the magnetization and θ is a small angle between the magnetic field \mathbf{H} and the easy axis \mathbf{c} of the sample. The field-induced polarization of the system is accompanied at 4.2 K by two successive steps in the torque, which lead to two well-defined maxima in the field-derivative of the torque at the first-order transitions fields $H_{2,3} \approx 25.5$ T and $H_c \approx 26$ T. Our torque data are in good agreement with our magnetostriction data (see Section IV), and also with magnetization measurements performed by Settai et al.² and Abe et al.³, in which two first-order transitions were reported at similar magnetic fields. From Fig. 4, it is clear that the two transitions $H_{2,3}$ and H_c merge at about 20 K into a single first-order transition H_c . We note that $H_{2,3}$ and H_c were found to be distinct up to 24 K in the magnetization data from Settai et al.². In our data, a first-order like anomaly at H_c can be seen up to 23 K. This is characterized by a symmetric positive anomaly in the field-derivative of the torque (Fig. 4). For $T \geq 24$ K, an asymmetric step-like anomaly as opposed to the symmetric maximum observed at lower temperatures is observed at H_c in the field-derivative of the torque. This anomaly indicates that the transition is of second-order⁹.

VI. RESISTIVITY

Fig. 5 shows measurements of the resistivity ρ_{xx} versus H of CeRh_2Si_2 for magnetic fields up to 50 T and temperatures between 1.5 K and 80 K. At low temperatures, a step-like anomaly is observed at the critical field $\mu_0 H_c = 25.9$ T (H_c is defined at the extremum of slope of $\rho_{xx}(H)$). This anomaly corresponds to the antiferromagnetic-to-paramagnetic borderline of the system. Our resistivity data show only one first-order tran-

sition to the polarized regime, while torque and magnetostriction data permitted us to observe two successive transitions at $H_{2,3}$ and H_c (Sections IV and V). The strong change of resistivity between the antiferromagnetic and the polarized phases is associated with a reconstruction of the Fermi surface as recently detected by quantum oscillations in measurements of the torque in high static magnetic fields¹³. The transition field H_c decreases with increasing temperature and reaches zero at $T_N(H = 0) = 36$ K. Below 20 K, the anomaly at H_c has an asymmetric step-like shape and can be considered as the signature of a first-order transition. At 20 K, the shape of $\rho_{xx}(H)$ is almost symmetric and a change of slope at a magnetic field of around 24 T has replaced the step-like anomaly observed at low temperature. For $20 \leq T \leq 36$ K, a second-order-like change of slope of $\rho_{xx}(H)$ can be defined at the antiferromagnetic transition field H_c . The ρ_{xx} versus H data plotted in Fig. 5 indicate that, at around (24 T, 20 K), the antiferromagnetic-to-paramagnetic transition in CeRh_2Si_2 goes from first-order at low temperature to second-order at high temperature. For $T > 36$ K, a broad maximum of $\rho_{xx}(H)$ is found at a magnetic field H_{pol} , which increases with T . This anomaly is attributed to the crossover between the low-field paramagnetic regime, where antiferromagnetic correlations dominate, and the high-field polarized paramagnetic regime. The initial positive slope of the magnetoresistivity is attributed to antiferromagnetic correlations. The persistence of a positive slope in $\rho_{xx}(H)$ at 80 K implies that antiferromagnetic correlations develop above 80 K. If the Ce ions would be independent, i.e., only subject to single-site phenomena as in the Kondo effect, a negative slope of the magnetoresistivity would be expected at all magnetic fields.

The derivative of the resistivity $\partial\rho_{xx}/\partial(\mu_0 H)$ is plotted in Fig. 6 for $\mu_0 H \leq 30$ T and $1.5 \leq T \leq 36$ K. Below 10 K, a well-defined minimum of $\partial\rho_{xx}/\partial(\mu_0 H)$

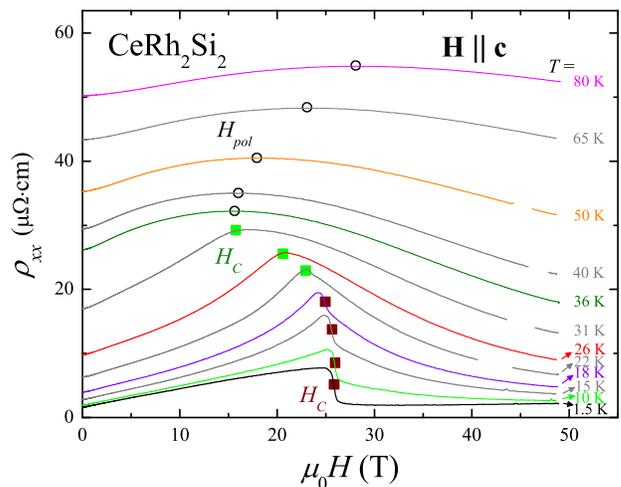


FIG. 5. (Color online) Resistivity ρ_{xx} versus magnetic field H in CeRh_2Si_2 , for $\mathbf{H} \parallel \mathbf{c}$ and $1.5 \leq T \leq 80$ K.

is obtained at the first-order transition field H_c . For $T > 10$ K, the size of the first-order-like anomaly in $\partial\rho_{xx}/\partial(\mu_0H)$ decreases with increasing T , being progressively replaced by a step-like anomaly in $\partial\rho_{xx}/\partial(\mu_0H)$. Between 26 K and 36 K, a clear step-like anomaly is observed in $\partial\rho_{xx}/\partial(\mu_0H)$ at H_c , which is defined at the extremum of slope of $\partial\rho_{xx}/\partial(\mu_0H)$. This step coincides with the second-order nature of the transition. The fact that both kinds of anomalies, i.e., a step and a minimum, can be defined in all $\partial\rho_{xx}/\partial(\mu_0H)$ versus H curves for $10 \leq T \leq 24$ K shows that the change between the low- and the high-temperature regimes is not so well-defined in our resistivity data. To understand these features, it would be interesting to investigate the transport properties of other systems where a magnetic transition also goes from second- to first-order when the temperature is lowered. The size of the step in $\partial\rho_{xx}/\partial(\mu_0H)$ reaches a maximum at $T = 20$ K, which may be related to enhanced magnetic fluctuations at around (24 T, 20 K), their intensity decreasing below 20 K when the transition becomes first-order. In Fig. 6, an additional anomaly can be observed in $\partial\rho_{xx}/\partial(\mu_0H)$ at the magnetic field $H_{1,2}$, for the temperatures $20 \leq T \leq 24$ K. This anomaly corresponds to the transition between the antiferromagnetic states AF1 and AF2, which occurs at $T_{1,2} = 26$ K in zero-field. Since $T_{1,2}$ is a first-order transition, an extremum of $\partial\rho_{xx}/\partial(\mu_0H)$, similarly to the one observed at H_c , should be expected at $H_{1,2}$. A first-order-like anomaly at $H_{1,2}$ was obtained by Levy et al. using static high magnetic fields¹³, but this anomaly is probably hidden here by a broadening of the transition due to the pulsed

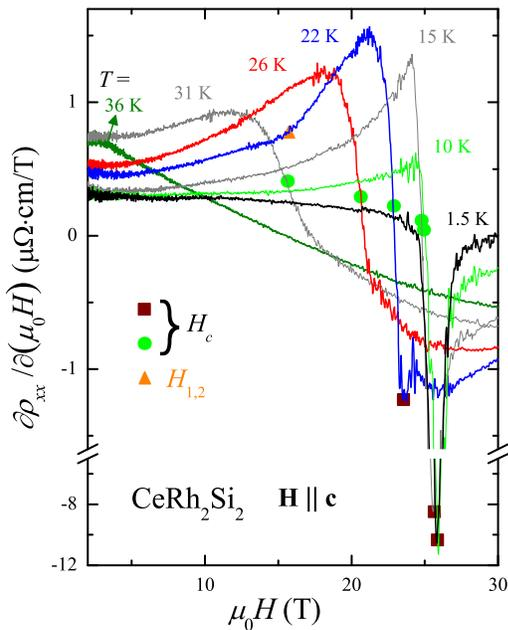


FIG. 6. (Color online) Magnetic field-derivative of the resistivity $\partial\rho_{xx}/\partial(\mu_0H)$ versus H in CeRh_2Si_2 for $\mathbf{H} \parallel \mathbf{c}$ and $1.5 \leq T \leq 36$ K.

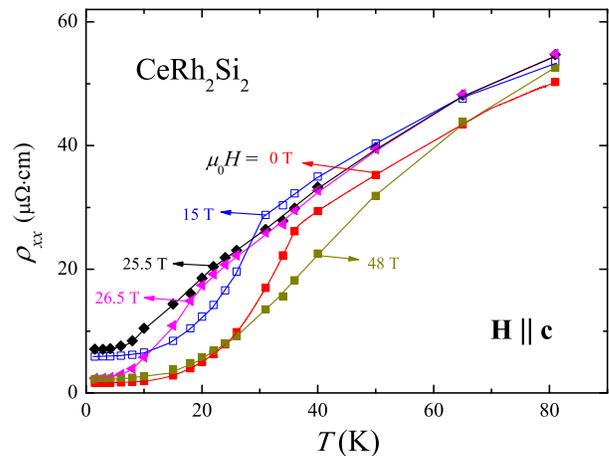


FIG. 7. (Color online) Resistivity versus temperature $\rho_{xx}(T)$ of CeRh_2Si_2 , for magnetic fields $\mathbf{H} \parallel \mathbf{c}$ of 0, 15, 25.5, 26.5 and 48 T.

nature of the magnetic field.

Fig. 7 shows the temperature dependence of ρ_{xx} at different magnetic fields. The curve at zero-field was measured separately, while the data in magnetic field have been extracted from the ρ_{xx} versus H data plotted in Fig. 5. No anomaly is seen at 25.5 T in contrast with the clear kinks at 36 K and 25 K in zero-field and at 15 T, respectively, which correspond to the transition line T_N (cf. the phase diagram in Fig. 1). However, the T -dependence of ρ_{xx} under 25.5 T over the wide T -window from above 20 K down to low temperatures looks quite anomalous. At low temperature, ρ_{xx} drops suddenly through H_c and the system becomes highly polarized paramagnetically. Plots of ρ_{xx} versus T^2 are shown in Fig. 8 (a) for magnetic fields below 25 T and in Fig. 8 (b) for magnetic fields above 25.5 T. In these plots, the dotted lines correspond to the fits to the data by $\rho_{xx} = \rho_{xx}^0 + AT^2$ made for $T \leq 8$ K. In Fig. 8 (c), the quadratic coefficient A and the low-temperature resistivity ρ_{xx}^0 extracted from the fits are presented. The step-like anomaly in ρ_{xx}^0 of course governs the behavior of ρ_{xx} at very low temperature (Fig. 5). A step-like anomaly was also reported in the ρ_{xx} versus p data at a critical pressure of around 10 kbar corresponding to the quantum phase transition to a paramagnetic regime^{1,8}. In the low-field antiferromagnetic state, quantum oscillations and band calculations based on the $4f$ -localized model have shown that the Fermi surface is multiple connected⁶. Thus, the orbital magnetoresistance is expected to be saturated and field-independent, at least below the critical field H_c . A Fermi surface reconstruction probably occurs at H_c , as indicated by the sudden variation of ρ_{xx}^0 . The slight increase of ρ_{xx}^0 observed above H_c (see Fig. 8 (c)) could result from an orbital effect due to a reconstruction of the Fermi surface in closed orbits at high fields. To support this hypothesis, the high-field condition $\omega_c\tau > 1$, where ω_c is the cyclotron frequency and τ the lifetime of the electron, should be fulfilled. This could be the case here, since the

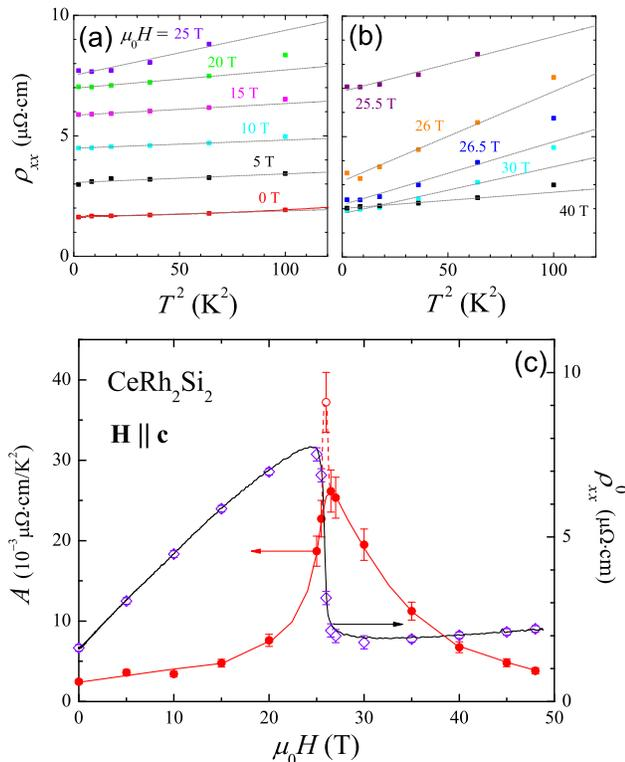


FIG. 8. (Color online) Resistivity of CeRh_2Si_2 in a ρ_{xx} shown versus T^2 , for $\mathbf{H} \parallel \mathbf{c}$ and a) $H \leq 25$ T, b) $H \geq 25.5$ T. Dotted lines correspond to fits to the data, for $T \leq 8$ K, by $\rho_{xx} = \rho_{xx}^0 + AT^2$. c) Plots of the quadratic coefficient A and of the residual resistivity ρ_{xx}^0 as a function of H . Red closed circles show the coefficient A extracted for $H \neq H_c$ (where a quadratic fit sounds reasonable), while a red open circle is used for A extracted at H_c (where a quadratic fit is probably not justified). The errors bars come from the uncertainty in the numerical fits to the data. Red (full and dotted) lines are guides to the eyes for the field variation of A . The black line shows the field-dependence of ρ_{xx} measured at 1.5 K.

value of $\rho_{xx}^0 \simeq 1.6 \mu\Omega \cdot \text{cm}$ at zero-field obtained on our sample is not so far from the value of $1.3 \mu\Omega \cdot \text{cm}$ measured on the sample studied in Ref. 6, for which quantum oscillations were reported at 30 mK. On the other hand, the increase of the magnetoresistivity observed above 30 T does not follow a clear $\Delta\rho/\rho \sim (\omega_c\tau)^2 \sim H^2$ behavior, so that the high-field condition $\omega_c\tau > 1$ could also be not yet fulfilled. Positive magnetoresistivity could also result from disorder effects as described in Ref. 14. Further experiments on samples of different qualities are required to solve this problem. A maximum of A is obtained at the transition $\mu_0 H_c = 26$ T to the polarized regime. The maximal value of A , which is a factor 15 bigger than the one found at zero magnetic field, is probably affected by the sudden step in ρ_{xx}^0 in the narrow region around H_c . A Fermi surface reconstruction presumably controls this step, around which the resistivity might not be dominated by the collisions of the quasiparticles. Thus, the close region around H_c might not be described within

the Kadowaki-Woods approach¹⁵. A Kadowaki-Woods approach is appropriate only when inelastic scattering processes, i.e., mechanisms related to the magnetic fluctuations of the f -electron moments in heavy-fermion systems, dominate the electronic effective mass and control the temperature dependence of the resistivity. Here the A coefficient might be proportional to the square root of the average effective mass only in magnetic fields below 25.5 T or above 26 T, assuming that the carrier density does not vary significantly. In these field ranges, A passes through a broad maximum at H_c , being 10 times bigger than its value at zero magnetic field. Resistivity data are thus consistent with an enhancement of the heavy-fermion effective mass by a factor of 3 at H_c . Because of this factor 3, fits close to H_c should have been made in a temperature window 3 times smaller than the fit made at zero-field. However, our sensitivity in pulsed magnetic fields does not allow to perform such an analysis.

VII. DISCUSSION

As shown in Fig. 8 (c), the H -enhancement of A occurs over a broad magnetic field window, of about 10 T, while the two transitions at $H_{2,3}$ and H_c are only separated by 0.5 T. Their experimental width is less than 0.1 T through the first-order metamagnetic transitions. A further comparison of the pressure^{8,12} and magnetic field-variations of A/A_{max} , as a function of $(p - p_c)/p_c$ and $(H - H_c)/H_c$ (see Fig. 9), leads to the remarkable result that their variations are almost comparable. Because the A coefficient extracted at 26 T (see Fig. 8) is surely affected by the sudden variation of ρ_{xx}^0 between 25.5 and 26 T it is not included in Fig. 9 (as well as in Fig. 11).

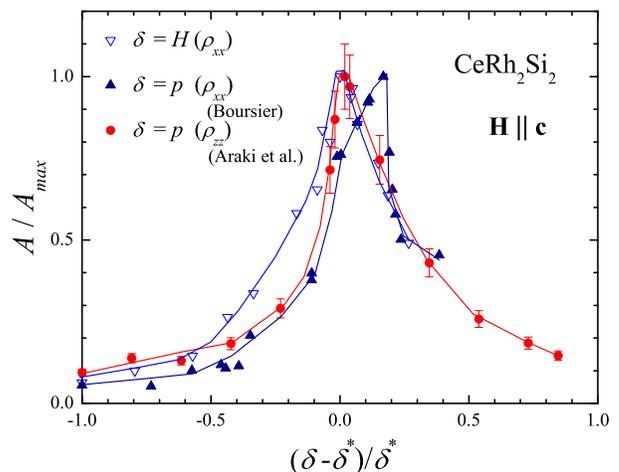


FIG. 9. (Color online) Comparison of the magnetic field- and pressure-dependences^{8,12} of the normalized quadratic coefficient A/A_{max} of the low-temperature resistivity of CeRh_2Si_2 versus $(\delta - \delta^*)/\delta^*$. δ is the magnetic field or the pressure and δ^* its critical value.

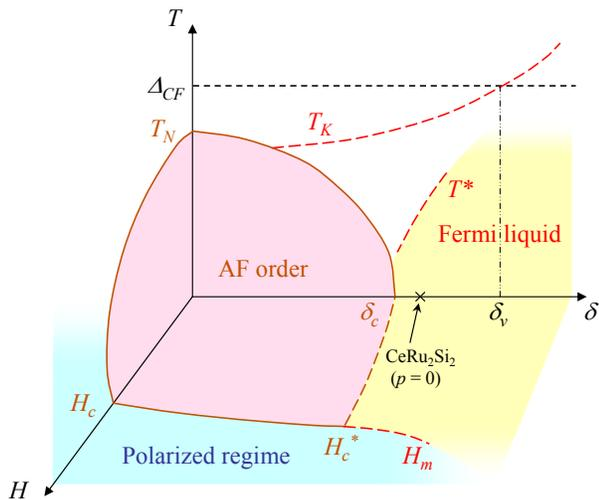


FIG. 10. (Color online) Schematic magnetic field-pressure or doping-temperature phase diagram of the prototypical heavy-fermion system CeRu_2Si_2 , when a magnetic field is applied along \mathbf{c} .

A similarity between the critical values reached at p_c and H_c has already been observed in the well-documented heavy-fermion series CeRu_2Si_2 , which is composed of Ising-type magnetic centers on the cerium sites, and where quantum criticality can be reached via lanthanum doping (fictitious negative pressure) or via pressure tuning. The (T, δ, H) phase diagram of CeRu_2Si_2 is represented schematically in Fig. 10, where δ is either the La-doping content x or the pressure p . At $H = 0$ a magnetic singularity separates the antiferromagnetic and paramagnetic ground states at δ_c . This corresponds to an effective negative pressure $p_c = -3$ kbar or a La-doping $x_c = 7.5$ % applied on the parent compound CeRu_2Si_2 (Ref. 16 and 17). δ_v corresponds to a pressure $p_v \simeq 2 - 5$ GPa applied on the parent compound. Above p_v the system is expected to enter into an intermediate valent regime²¹. From the antiferromagnetic phase, application of a magnetic field along \mathbf{c} induces a first-order metamagnetic transition at H_c , which leads to a critical magnetic field end-point $H_c^* \simeq 4$ T at δ_c (Ref. 18). Above δ_c , a sharp pseudo-metamagnetic crossover occurs at a magnetic field H_m , which reaches 8 T in pure CeRu_2Si_2 at ambient pressure. Using inelastic neutron scattering, it has been demonstrated that the crossing through H_m is associated with the collapse of the antiferromagnetic correlations together with an enhancement of the low-energy ferromagnetic fluctuations in a quite narrow field-range^{19,20}. The transition at x_c is associated with an enhancement of the antiferromagnetic fluctuations¹⁷. A key observation is the increase by 50 % of the average effective mass at H_m , by comparison to the zero-field value, as measured by the linear T -term γ of the specific heat²². Above H_m , the effective mass decreases strongly with H .

Table I recapitulates for CeRh_2Si_2 and CeRu_2Si_2 , the

residual values of the linear T -term γ of the specific heat at $(H = 0, p = 0)$, $(H_{m,c}, p = 0)$, and $(H = 0, p_c)$ (for CeRu_2Si_2 , p_c corresponds to a La-doping $x_c = 7.5$ %). The value of the initial susceptibility χ_c^0 along the easy axis \mathbf{c} as well as the ratio χ_c^0/χ_a^0 of the susceptibilities χ_c^0 and χ_a^0 along \mathbf{c} and along \mathbf{a} , respectively, are also summarized in Table I. Typically, γ and χ_c^0 are 10 times bigger in CeRu_2Si_2 (Ref. 18 and 23) than in CeRh_2Si_2 (Ref. 24 and 25), which indicates the presence of more intense low-temperature magnetic fluctuations. This leads to an effective mass 10 times bigger in CeRu_2Si_2 than in CeRh_2Si_2 . The anisotropy of the magnetic susceptibility, estimated via the ratio χ_c^0/χ_a^0 , is also 10 times bigger in CeRu_2Si_2 than in CeRh_2Si_2 . The proximity of CeRh_2Si_2 to a valence instability could explain both the reduction of the magnetic anisotropy, via a Kondo broadening/overlapping of the crystal-field levels, and the reduction of the saturated moment of this system². In such a scenario, the stronger magnetic fluctuations in CeRu_2Si_2 could be a consequence of a stronger magnetic anisotropy. Finally, $\gamma(H_{m,c}, p = 0)$ and $\gamma(H = 0, p_c)$ are comparable in both CeRu_2Si_2 and CeRh_2Si_2 (see Table I). This indicates that the mechanisms which control the magnetic field- and pressure-enhancements of γ , and thus of the average effective masses (within a Fermi liquid picture) might be closely connected. This conclusion is compatible with the variations of A/A_{max} as a function of $(p - p_c)/p_c$ and $(H - H_c)/H_c$ reported in Fig. 9.

In Fig. 11, a comparison is made, for CeRh_2Si_2 and CeRu_2Si_2 between the variations of A/A_{max} with the reduced magnetic field $(H - H^*)/H^*$ when $\mathbf{H} \parallel \mathbf{c}$ ($H^* = H_c$ for CeRh_2Si_2 and $H^* = H_m$ for CeRu_2Si_2). Below H^* , A/A_{max} increases faster with $(H - H^*)/H^*$ in CeRh_2Si_2 than in CeRu_2Si_2 . Oppositely, above H^* A/A_{max} decreases faster in CeRu_2Si_2 than in CeRh_2Si_2 . In a conventional magnetic fluctuations scenario²⁸⁻³⁰, an enhancement of the magnetic order parameter fluctuations controls both A and γ , which leads to a strong effective mass related to a fixed Kadowaki-Woods ratio A/γ^2 (Ref. 15). In real systems, A and γ can be sensitive to other effects, such as the nature of the magnetic fluctuations (antiferromagnetic, ferromagnetic, single-site etc.) and departures from a unique Kadowaki-Woods ratio can be the consequence of a wavevector dependence of the mag-

TABLE I. Specific heat linear coefficient γ at $(H = 0, p = 0)$, $(H_{m,c}, p = 0)$, $(H = 0, p_c)$, low temperature susceptibility χ_c^0 along \mathbf{c} , and ratio χ_c^0/χ_a^0 of the susceptibilities along \mathbf{c} and \mathbf{a} , for CeRh_2Si_2 and CeRu_2Si_2 .

| | CeRh_2Si_2 | CeRu_2Si_2 |
|---|----------------------------|----------------------------|
| $\gamma(H = 0, p = 0)$ (mJ/mol.K ²) | 23 [24] | 350 [18] |
| $\gamma(H_{m,c}, p = 0)$ (mJ/mol.K ²) | 40 [13] | 550 [22] |
| $\gamma(H = 0, p_c)$ (mJ/mol.K ²) | 80 [24] | 600 [26] |
| χ_c^0 (10 ⁻³ emu/mol) | 3 [25] | 36 [23] |
| χ_c^0/χ_a^0 | 1-5 [25] | 10-20 [23] |

TABLE II. Lattice parameters a and c , unit cell volume V , and characteristic energy scales T_N , T_K , T_{corr} , and Δ_{CF} for CeRh_2Si_2 and CeRu_2Si_2 .

| | CeRh_2Si_2 | CeRu_2Si_2 |
|-----------------------|----------------------------|----------------------------|
| T_N (K) | 36 | - |
| T_K (K) | 35 [35] | 25 [17] |
| T_{corr} (K) | > 80 | 50-80 [32,33,34] |
| Δ_{CF} (K) | 300 [35] | 200 [35] |
| a (Å) | 4.09 [36] | 4.19 [36] |
| c (Å) | 10.18 [36] | 9.78 [36] |
| V (Å ³) | 170.6 [36] | 171.7 [36] |

netic fluctuations. In high magnetic fields, the persistence of the proportionality between A and γ^2 has been verified for CeRu_2Si_2 (Ref. 31). The differences between CeRu_2Si_2 and CeRh_2Si_2 shown in Fig. 11 might be connected to the differences of their magnetic fluctuation spectra. In both systems, the low-field variations of $A(H)$ are believed to be governed by antiferromagnetic fluctuations. Fig. 11 is compatible with the expectation that antiferromagnetic fluctuations are less important in CeRh_2Si_2 , which is ordered antiferromagnetically with a relatively high T_N than in CeRu_2Si_2 , which is a paramagnet close to an antiferromagnetic instability. As in CeRu_2Si_2 (ref. 19 and 20), critical ferromagnetic fluctuations might play a role in CeRh_2Si_2 for the enhancement of A and γ in a narrow field range around H^* . High above H^* , for CeRh_2Si_2 $A(H)$ is still enhanced and its slope remains important up to rather high magnetic fields. This might be related to additional energy scales, such as the Kondo temperature.

A comparison of the magnetic energy scales of CeRh_2Si_2 and CeRu_2Si_2 is presented in Table II. In

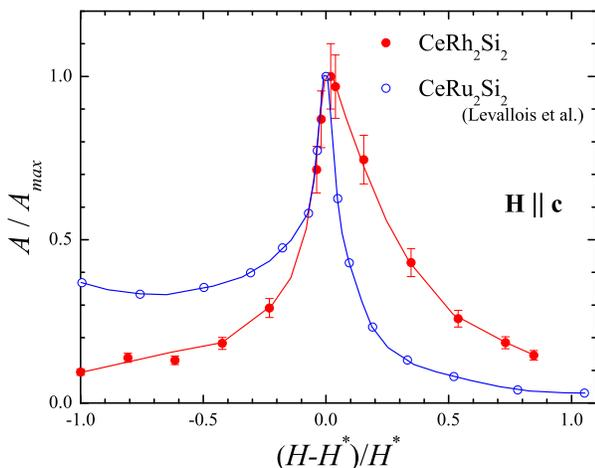


FIG. 11. (Color online) Comparison of the magnetic field dependences of the quadratic coefficient A of the low-temperature resistivity, in a A/A_{max} versus $(H-H^*)/H^*$ plot, for the heavy fermions CeRh_2Si_2 and CeRu_2Si_2 (Ref. 27).

CeRu_2Si_2 , antiferromagnetic correlations were evidenced by inelastic neutron scattering up to a temperature T_{corr} estimated between 50 K and 80 K^{32,33}. This can be connected to the initial positive slope of the magnetoresistivity observed for $T \leq 50$ K³⁴. Similarly, the initial positive slope of $\rho_{xx}(H)$ observed up to 80 K in CeRh_2Si_2 (see Fig. 5) is believed to be a manifestation of the strength of the antiferromagnetic correlations. We note that, if the Ce ions behave as independent paramagnetic centers, assuming that the orbital magnetoresistance can be neglected, the slope of the magnetoresistivity would be negative. In CeRh_2Si_2 , the onset of antiferromagnetic correlations is established at a temperature T_{corr} higher than 80 K, i.e., higher than in CeRu_2Si_2 . Table II also shows that, while the unit cell volumes of CeRh_2Si_2 and CeRu_2Si_2 are similar, their lattice parameters are quite different. The bigger inter-plane distance between the Ce ions could be a reason for stronger RKKY antiferromagnetic correlations in CeRh_2Si_2 . Indeed, the initial decrease of T_N under pressure is mainly driven by the reduction of the lattice parameter c . More precisely, the anomaly at T_N in the thermal expansion along c is negative and 6 times bigger than the one along a (see Ref. 2 and Section IV). This indicates that the initial slope of T_N versus uniaxial pressure is 6 times bigger for an uniaxial pressure along c than along a . At ambient pressure, the Kondo temperature of CeRh_2Si_2 is generally estimated at around 35 K^{35,36}, which is 50 % higher than in CeRu_2Si_2 (see Table II). The origin of antiferromagnetism in CeRh_2Si_2 is related to the strength of T_{corr} by comparison to T_K . A smaller T_{corr}/T_K in CeRu_2Si_2 might explain why this system is paramagnetic. In addition, CeRh_2Si_2 is probably close to a mixed valence regime. This is indicated by the smallness of its Sommerfeld coefficient γ , which reaches only 80 mJ/mol.K² at the critical pressure p_c , and of its small pressure dependence (Ref. 24). The value of γ at p_c in CeRh_2Si_2 is rather similar to that of typical mixed-valence compounds, e.g. $\gamma \simeq 40$ mJ/mol.K² in CeSn_3 (Ref. 37). Also, the drop of the magnetic anisotropy in CeRh_2Si_2 (Ref. 25) might be related to a broadening of the crystal-field levels due to a strong enhancement of T_K when entering into the valence intermediate regime. A unique property of CeRh_2Si_2 is that its ordering temperature is strongly pressure dependent since the rather high value of $T_N = 36$ K at ambient pressure is driven to zero at a "relatively small" pressure $p_c = 11$ kbar. The strong pressure-dependence of T_N close to p_c could be due to a strong increase of T_K under pressure because of the proximity to a valence transition p_v . Knowing that H_c reaches 36 T at p_c in CeRh_2Si_2 (Ref. 38) one can further speculate if, for pressure bigger than p_c and p_v , a magnetic field could push the system to a valence critical point (as discussed in Ref. 39). In such case, a study of the variations of A approaching and through the field-induced valence critical point would give important clues about the formation of quasiparticles in heavy-fermion and intermediate-valent systems.

VIII. CONCLUSION

A study of the heavy-fermion antiferromagnet CeRh_2Si_2 has been performed in high magnetic fields of up to 50 T. From resistivity, torque, magnetostriction, and thermal expansion measurements we deduced its magnetic field-temperature phase diagram. It is composed of at least three distinct antiferromagnetic phases and possibly of a tetra-critical point. Fits of our resistivity data showed i) a large H -window where the quadratic coefficient A is enhanced, in contrast to the sharpness of the metamagnetic transitions, and ii) that similar values are obtained for $A(p=0)/A(p_c)$ and $A(H=0)/A(H_c)$. This implies that both pressure- and magnetic field-induced criticalities might be controlled by common features, although they are expected to be governed by an-

tiferromagnetic and ferromagnetic fluctuations, respectively. For both pressure- and field-induced magnetic instabilities the effective mass is not found to diverge. Finally, the drop of the resistivity observed at H_c is compatible with the recent observation of a Fermi surface reconstruction at H_c , possibly related to a large decoupling between the majority and minority spin band.

ACKNOWLEDGMENTS

We thank M. Nardone, A. Zitouni, and J. Béard for experimental support, A. Demuer and I. Sheikin for discussions and for showing us data prior to publication, and L. Malone for carefully reading the manuscript. This work was supported by the French ANR Delice and by Euro-magnet II via the EU contract RII3-CT-2004-506239.

-
- ¹ M. Ohashi, G. Oomi, S. Koiwai, M. Hedo, and Y. Uwatoko, *Phys. Rev. B* **68**, 144428 (2003).
 - ² R. Settai, A. Misawa, S. Araki, M. Kosaki, K. Sugiyama, T. Takeuchi, K. Kindo, H. Haga, E. Yamamoto, and Y. Ōnuki, *J. Phys. Soc. Jpn.* **66**, 2260 (1997).
 - ³ H. Abe, H. Suzuki, H. Kitazawa, T. Matsumo, and G. Kido, *J. Phys. Soc. Jpn.* **66**, 2525 (1997).
 - ⁴ T. Graf, M.F. Hundley, R. Modler, R. Movshovich, J.D. Thompson, D. Mandrus, R.A. Fisher, and N.E. Phillips, *Phys. Rev. B* **57**, 7442 (1998).
 - ⁵ S. Kawarazaki, M. Sato, Y. Miyako, N. Chigusa, K. Watanabe, N. Metoki, Y. Koike, and M. Nishi, *Phys. Rev. B* **61**, 4167 (2000).
 - ⁶ S. Araki, R. Settai, T.C. Kobayashi, H. Harima, and Y. Ōnuki, *Phys. Rev. B* **64**, 224417 (2001).
 - ⁷ R. Movshovich, T. Graf, D. Mandrus, J. D. Thompson, J. L. Smith, and Z. Fisk, *Phys. Rev. B* **53**, 8241 (1996).
 - ⁸ S. Araki, M. Nakashima, R. Settai, T. Kobayashi, and Y. Ōnuki, *J. of Phys.: Condens. Matter* **14**, L377 (2002).
 - ⁹ A first-order transition is characterized by a step-like anomaly in the first-derivatives of the free energy, as the entropy, the length, and the magnetization. Subsequently, it is accompanied by a symmetric and sharp extremum, at which the transition temperature or field can be defined, in the second-derivatives of the free energy, as the specific heat, the thermal expansion and magnetostriction coefficients, and the field-derivative of the magnetization (or torque). A second-order transition is characterized by a step-like anomaly in the second-derivatives of the free energy - the transition temperature or field can be defined at the extremum of slope, generally at the half of the step.
 - ¹⁰ S. Araki, A. Misawa, R. Settai, T. Takeuchi, and Y. Ōnuki, *J. Phys. Soc. Jpn.* **67**, 2915 (1998).
 - ¹¹ A. Villaume, D. Aoki, Y. Haga, G. Knebel, R. Boursier, and J. Flouquet, *J. Phys.: Condens. Matter* **20**, 015203 (2007).
 - ¹² R. Boursier, PhD-thesis, Université Joseph Fourier, Grenoble (2005).
 - ¹³ F. Levy, A. Demuer, I. Sheikin et al, to be published.
 - ¹⁴ F.J. Ohkawa, *Phys. Rev. Lett.* **64**, 2300 (1990).
 - ¹⁵ K. Kadowaki and S.B. Woods, *Solid State Commun.* **58**, 507 (1986).
 - ¹⁶ P. Haen, F. Lapierre, J. Voiron, and J. Flouquet, *J. Phys. Soc. Jpn* **65** (Suppl. B), 27 (1996).
 - ¹⁷ W. Knafo, S. Raymond, P. Lejay, and J. Flouquet, *Nature Physics* **5**, 753 (2009).
 - ¹⁸ R.A. Fisher, C. Marcenat, N.E. Phillips, P. Hean, F. Lapierre, P. Lejay, J. Flouquet, and J. Voiron, *J. Low Temp. Phys.* **84**, 49 (1991).
 - ¹⁹ M. Sato, Y. Koike, S. Katano, N. Metoki, H. Kadowaki, and S. Kawarasaki, *J. Phys. Soc. Jpn.* **70** Suppl. A, 118 (2001).
 - ²⁰ J. Flouquet, Y. Haga, P. Haen, D. Braithwaite, G. Knebel, S. Raymond, and S. Kambe, *J. Magn. Magn. Mat.* **272-276**, 27 (2004).
 - ²¹ K. Payer, P. Haen, J.-M. Laurant, J.-M. Mignot, and J. Flouquet, *Physica B* **186-188**, 503 (1993).
 - ²² C. Paulsen, A. Lacerda, L. Puech, P. Lejay, J.L. Tholence, J. Flouquet, and A. de Visser, *J. Low Temp. Phys.* **81**, 317 (1990).
 - ²³ P. Haen, F. Lapierre, P. lejay, and J. Voiron, *J. Magn. Magn. Mat.* **116**, 108 (1992).
 - ²⁴ T. Graf, J.D. Thompson, M.F. Hundley, R. Movshovich, Z. Fisk, D. Mandrus, R.A. Fisher, and N.E. Phillips, *Phys. Rev. Lett.* **78**, 3769 (1997).
 - ²⁵ H. Mori, N. Takeshita, N. Mori, and Y. Uwatoko, *Physica B* **259-261**, 58 (1999).
 - ²⁶ S. Raymond, W. Knafo, J. Flouquet, and P. Lejay, to be published (arXiv:0909.4729v1 [cond-mat.str-el]).
 - ²⁷ J. Levallois, K. Behnia, J. Flouquet, P. Lejay, and C. Proust, *Europhys. Lett* **85**, 27003 (2009).
 - ²⁸ J.A. Hertz, *Phys. Rev. B* **14**, 1165 (1976).
 - ²⁹ A.J. Millis, *Phys. Rev. B* **48**, 7183 (1993).
 - ³⁰ T. Moriya and T. Takimoto, *J. Phys. Soc. Jpn.* **64**, 960 (1995).
 - ³¹ R. Daou, C. Bergemann, and S.R. Julian, *Phys. Rev. Lett.* **96**, 026401 (2006).
 - ³² L.P. Regnault, J.L. Jacoud, J.M. Mignot, J. Rossat-Mignod, C. Vettier, P. lejay, and J. Voiron, *Physica B* **163**, 606 (1990).

- ³³ S. Raymond, W. Knafo, J. Flouquet, and P. Lejay, *J. Low Temp. Phys.*, **147**, 215 (2007).
- ³⁴ P. Haen, J. Flouquet, F. Lapierre, P. lejay, J.M. Mignot, A. Ponchet, and J. Voiron, *J. Magn. Magn. Mat.* **63-64**, 320 (1987).
- ³⁵ V. Vildosola, A.M. Llois, and M. Alouani, *Phys. Rev. B* **71**, 184420 (2005).
- ³⁶ A. Severing, E. Holland-Moritz, and B. Frick, *Phys. Rev. B* **39**, 4164 (1989).
- ³⁷ R. Takke, M. Nicksch, W. Assmus, B. Lüthi, R. Pott, R. Schefzyk, and D.K. Wohlleben, *Z. Phys. B* **44**, 33 (1981),
- J.R. Cooper, C. Rizzuto, G. Olcese, *J. Phys. (Paris) C* **1-32**, 1136, (1971).
- ³⁸ H. Hamamoto, K. Kindo, T.C. Kobayashi, Y. Uwatoko, S. Araki, R. Settai, and Y. Onuki, *Physica B* **281-282**, 64 (2000).
- ³⁹ S. Watanabe, A. Tsuruta, K. Miyake, and J. Flouquet, *J. Phys. Soc. Jpn.* **78**, 104706 (2009).